Improving postfire soil burn severity mapping with hyperspectral unmixing

Peter R. Robichaud[1], Sarah A. Lewis[1*], Denise M. Laes[2],
Andrew T. Hudak[1], Raymond F. Kokaly[3], and Joseph A. Zamudio[4]

[1]*Rocky Mountain Research Station, US Department of Agriculture Forest Service, Moscow, Idaho, USA*
[2]*Remote Sensing Applications Center, US Department of Agriculture Forest Service, Salt Lake City, Utah, USA*
[3]*Spectroscopy Laboratory, US Department of the Interior Geological Survey, Denver, Colorado, USA*
[4]*Applied Spectral Imaging Boulder, Colorado, USA*

Short title: Postfire burn severity mapping

Summary: Soil surface burn severity mapping is improved using spectral unmixing of hyperspectral imagery after the Hayman Fire, Colorado.

Submitted to: Photogrammetric Engineering and Remote Sensing (30 September 2005)

Abstract

The capabilities of high resolution hyperspectral imagery were investigated to discriminate fine-scale postfire ground cover components after the 2002 Hayman Fire. Four spectral endmembers (ash, soil, scorched and green vegetation) were used in a Mixture Tuned Matched Filtering partial spectral unmixing process. From 72 validation field plots, the ground measures of each endmember were found to be significantly related to the corresponding matched filter (MF) scores. Vegetation measures were more strongly correlated to the MF scores (green vegetation [r=0.51, p-value <0.0001] and scorched vegetation [r=0.55, p-value <0.0001]) than surface cover measures (soil [r=0.40, p-value =0.0006] and ash [r=0.30, p-value =0.01]). However, soil surface effects were more accurately assessed with the fine-scale hyperspectral imagery than normalized burn ratio (NBR) values that are routinely used to create postfire burn severity maps.

Keywords: remote sensing, Hayman Fire, Mixture Tuned Matched Filter, NBR

1.0 Introduction

For decades, rehabilitation crews have mapped burn severity after wildfires in order to assess fire effects on the landscape. Postfire effects vary depending upon the pre-fire environment and the intensity and duration of the fire in a given location (Ryan and Noste, 1983; DeBano *et al*., 1998; Ryan, 2002; Ice *et al*., 2004; van Wagtendonk *et al*., 2004). Although a continuum of fire effects on the environment are evaluated to determine burn severity (Jain *et al*., 2004), it is generally mapped in discrete categories of low, moderate, and high, corresponding to the relative magnitude of change in the post-wildfire appearance of vegetation, litter and soil.

Potential watershed responses to wildfire, such as increased runoff, peak flows, and erosion, typically increase with increasing soil burn severity (DeBano, 2000; Robichaud, 2000; Moody and Martin, 2001; Moody *et al.*, 2005). As a result, postfire assessment and mapping of soil burn severity is crucial for rehabilitation decision-making. Areas that exhibit characteristics of high soil burn severity, such as deep soil charring (gray or orange soil color) and complete loss of vegetative cover, are at increased risk of soil erosion (Parsons, 2003; Lewis *et al*., in press). However, it has been argued recently that standard burn severity indices primarily reflect postfire canopy vegetation conditions and show little indication of soil burn severity (van Wagtendonk *et al*., 2004).

Burned Area Reflectance Classification (BARC) maps (RSAC, 2005) are created from multispectral satellite imagery such as MODIS (Moderate Resolution Imaging Spectroradiometer), SPOT (Systeme pour l'Observation de la Terre), or Landsat Thematic Mapper (TM) or Enhanced Thematic Mapper Plus (ETM+). TM and ETM+ are

often used because of two bands, the near-infrared band (4) and a mid-infrared band (7), which have been shown to be sensitive to fire-induced changes to vegetation and soil (Key and Benson, 2002; van Wagtendonk *et al*., 2004). Green vegetation is most highly reflective in the near-infrared range of the electromagnetic spectrum, while exposed mineral soil and rock are most reflective in the mid-infrared region; fire typically reduces the amount of green vegetation while increasing soil exposure (Patterson and Yool, 1998). A ratio of the reflectance values of the two bands, known as the Normalized Burn Ratio (NBR) provides an index of increasing burn severity (Key and Benson, 2002). A BARC map results from the classified NBR values: unburned, low, moderate or high burn severity (Parsons and Orlemann, 2002).

Digital elevation models and vegetation layers combined with classification rules are then used to create a preliminary Burned Area Emergency Rehabilitation (BAER) burn severity map (Parsons and Orlemann, 2002). Rehabilitation teams adjust this map based on observed severity conditions generally related to surface/soil conditions or vegetation mortality. Valuable time and resources are spent ground-truthing and correcting the preliminary BARC maps to produce an acceptable burn severity map (Hardwick *et al*., 1997; Patterson and Yool, 1998; Parsons, 2003; Clark *et al*., 2003). Without these improved modifications regarding specific resources at risk, a burn severity map has the potential to be used for unintended purposes. In order to accurately prescribe soil stabilization treatments to high erosion-risk areas, a burn severity map must represent the fire's effects on the soil surface.

Newer hyperspectral sensors garner high-resolution data that can distinguish a range of features beyond the scope of broadband satellite imagery and show promise for improving the direct measurement of soil burn severity (van Wagtendonk *et al*., 2004). Airborne hyperspectral sensors provide imagery in narrow bands of reflectance spectra arranged contiguously from the visible through the short-wave infrared (SWIR) range of the electromagnetic (EM) spectrum, approximately 400–2500 nm. The spectral resolution typically averages 15 nm bandwidths and the ground resolution (pixel size) of these remotely sensed images is as fine as 1 to 5 m, over an area of many square kilometers (sensor and altitude specific). The multidimensional image data is often referred to as a data cube; layers of contiguous wavebands over an area of interest. Field spectrometers provide even higher resolution data (1–2 nm bandwidths and sub-meter spatial sampling) for the same spectral range, and are used to correlate the reflectance from ground-surface features to remotely sensed imagery (Clark *et al*., 2002). van Wagtendonk *et al*. (2004) calculated a band ratio similar to the NBR with AVIRIS (Airborne Visible and Infrared Imaging Spectrometer) hyperspectral bands and showed that the ratio between narrower wavebands may be more sensitive to fire effects than traditional broadband ratios. This work suggested the advantages of the higher spatial resolution and materials discrimination power of hyperspectral imagery for postfire scenes.

Typically, a single image pixel is the sum of the individual reflectance spectra from a mixture of surface materials (Theseira *et al*., 2003; Song, 2005). This image retains some characteristic features of the individual spectra from each of the component reflective materials; however, they are diminished. Often, characteristic spectral features for a

specific material, such as mineral content of soil or vegetation type, are narrow—in the range of ten(s) of nanometers. The high information content of spectra extracted from hyperspectral imagery makes it possible to ‘unmix’ the characteristic spectral signatures, known as endmembers, of the individual reflecting materials that comprise each pixel. Once the endmembers are known, linear unmixing of individual pixels can determine the fractional component spectra and, in turn, the fractional component of the materials (Adams *et al*., 1986; Roberts *et al*., 1993).

Determining the component spectra of an image pixel requires high-quality reference spectra. These reference spectra can be obtained from existing spectral libraries, collected in situ with a field spectrometer, or extracted from the hyperspectral image (Song, 2005). To compare the image endmembers to library reflectance spectra, the image spectra must be from the surface material with as little additional spectral ‘noise’ as possible. Remote sensing instruments measure all upwelling radiance that arrives at the sensor. The more important factors determining radiance are solar irradiance, two-way atmospheric transmittance, atmospheric scattering, and reflectance from the surface materials (Gao *et al*., 1993; Analytical Imaging and Geophysics LLC, 2002). Image radiance data are converted to reflectance by eliminating the solar and atmospheric effects described above from the radiance signal. However, it may still be difficult to obtain a ‘pure’ image endmember spectral signature for a given material (Song, 2005).

It has been suggested that most land cover scenes can be mapped as endmember combinations of green vegetation, non-photosynthetic vegetation, soil and shade (Roberts *et al*., 1993; Adams *et al*., 1995; Theseira *et al*., 2003; Song, 2005). A combination of

these four endmembers along with ash and/or char endmembers would account for the majority of the cover types of a typical postfire scene. Lewis *et al*. (in press) found that percent exposed mineral soil and litter cover were the most indicative factors when measuring soil burn severity in the field. The ability to distinguish postfire ground characteristics at the sub-pixel scale will provide a better indication of the fire's effects on the soil and provide a more detailed and accurate assessment of the postfire conditions.

The goal of this study was to determine how remotely sensed hyperspectral data can be used to analyze and map postfire soil burn severity. The specific objectives were to: 1) use spectral mixture analysis of hyperspectral imagery to discriminate ground characteristics that are indicative of soil burn severity; 2) compare field measurements to the relative abundances of each endmember estimated from the spectral mixture analysis; and 3) develop a spectral library of soil burn severity endmembers to improve soil burn severity classification.

2.0 Study Area

In the summer of 2002, the Hayman Fire burned more than 55,000 ha within the South Platte River drainage on the Front Range of the Rocky Mountains between Denver and Colorado Springs, CO (Graham, 2003) (Figure 1). The South Platte River flows from southwest to northeast through the burned area, with the Cheesman Reservoir (a municipal water source) at risk for contamination via runoff and erosion. The long-term average annual precipitation is 400 mm at the Cheesman weather station (elevation 2100

m) (Colorado Climate Center, 2004). The region is underlain by the granitic Pikes Peak batholith, with frequent rock outcrops. The main soil types are Sphinx and Legault series, which are coarse-textured sandy loams, gravelly sandy loams and clay loams (Cipra *et al*., 2003; Robichaud *et al.*, 2003). The dominant tree species are ponderosa pine (*Pinus ponderosa*) and Douglas fir (*Pseudotsuga menziesii*) (Romme *et al*., 2003).

3.0 Data Acquisition

3.1 *Airborne Hyperspectral Imagery*

In late August 2002, fourteen adjacent flight lines of hyperspectral imagery were collected over the Hayman Fire by ESSI (Earth Search Sciences Inc., Kalispell, MT)[1] with an airborne "whisk-broom" Probe I sensor. Each flight line, or data cube, covered a track ~28 km long and 2.5 km wide; corresponding to a 512 pixel-wide swath with each georeferenced square pixel equal to ~25 m^2. The Probe I sensor received electromagnetic energy reflected from the surface in 128 contiguous spectral bands that spanned 432 to 2512 nm; the spectral resolution of each band was between 14 and 20 nm. An on-board global positioning system (GPS) and inertial measurement unit acquired geolocation data that were matched in time with the spectral data collection. The location data, together with 30-m digital elevation models, were used to generate Input Geometry (IGM) files, which were used post-image analysis to georeference the results.

[1] The use of trade or firm names in this publication is for reader information and does not imply endorsement by the U.S. Department of Agriculture Forest Service of any product or service.

3.2 Field Spectrometer Data

In July 2002, prior to the airborne acquisitions, field spectra were collected through cooperation with the U.S. Geological Survey, using their ASD (Analytical Spectral Devices, Boulder, CO) PRO-XR field spectroradiometer. The spectral range is 350 to 2500 nm, with a 2 nm spectral resolution that yields 256 contiguous spectral bands, spanning nearly the same range of the EM spectrum as ESSI's Probe I sensor used for the airborne imaging. The field spectrometer was calibrated against a spectralon panel immediately before field spectra were collected. The spectralon panel is a bright calibration target with well-documented reflectance in the 400 to 2500 nm region of the EM spectrum, and is used to convert relative reflectance to absolute reflectance. A spectralon absorption feature at 2130 nm was corrected before the field spectra were related to the image spectra.

Bright target ground-calibration field spectra were collected on the north shore of the Cheesman Reservoir, over bright, spectrally homogenous granitic rocks. The average spectrum was convolved to the bandwidth wavelengths of the Probe I sensor (Clark *et al*., 2002). In addition, field spectra from high and low burn severity sites were collected on the surface and, using an aerial lift truck, at the canopy level. The atmospheric conditions in which the burn severity field spectra were collected were too different from those present during the airborne data acquisition to directly relate the two data sets. However, the spectral characteristics of selected field spectra were used as a guide to identify and select image endmembers to generate the reference spectral libraries.

3.3 Field measurements

In July 2002, ‘ground truth’ validation data were collected at 183 sample plots with approximately 60 sample plots in each of the three burn severity classes (low, moderate, and high) as delineated by the BAER burn severity map. This burn severity map was created by the Remote Sensing Applications Center (RSAC) in 2002 from a SPOT image using the normalized burn ratio (NBR) (RSAC, 2005). East-west transects were located in visually homogenous areas at least 20 m from roads with approximately 9 sample plots per transect. Each sample plot consisted of a 4-m diameter circle in which 24 soil and vegetation variables were measured and a 7-m diameter circle in which tree condition and canopy measurements were made (details in Lewis *et al*., in press). The location of the center of each plot was recorded with a GPS device. Minor cover fractions, which were often grasses, forbs, shrubs, woody debris, stumps or rocks, were first estimated on each plot. A value of one percent was recorded if there was a trace of the material within the plot. The more common types of cover, which were exposed mineral soil, ash, litter and rock, were then estimated. The largest cover component was estimated last and the percent cover was forced to sum to 100%. The percent burned and degree of char (low, moderate or high) of each cover component was also estimated. For the purpose of correlating the ground measurements to the hyperspectral image, the vegetation constituents (both surface and canopy) were combined into three categories: green vegetation, non-photosynthetic vegetation and scorched vegetation.

3.4 Atmospheric correction of hyperspectral data

Atmospheric correction of the airborne hyperspectral imagery was accomplished using ACORN (Atmospheric CORrection Now) without any additional artifact suppression (Analytical Imaging and Geophysics, LLC, 2002). These non-smoothed reflectance data were further refined with a radiative transfer ground-controlled (RTGC) calibration. This involves calculating a multiplier from the differences between the mean image-reflectance spectrum over the area where bright target calibration field spectra were collected at Cheesman Reservoir and the corresponding average corrected field-reflectance spectrum. The multiplier was then applied to the ACORN corrected image-reflectance data. By applying the same multiplier, which is based on the atmospheric conditions present during the acquisition of flight line 7, to the other flight lines, variations in the atmosphere occurring due to the time differential between data acquisition were not all completely accounted for, but were believed to be negligible because all flight lines were acquired within a four hour time window (two hours on either side of local solar noon).

Two data cubes (flight lines 7 and 8) were initially delivered with missing ACORN-generated reflectance data. Once these data were provided, a comparison of ACORN reflectance spectra of the same geographic location on adjacent flight lines indicated that the first set of ACORN reflectance data was processed with different input parameters from the second set (lines 7 and 8). Because these lines contain pixels corresponding to the Cheesman Reservoir ground calibration site, a separate RTGC calibration was performed and a different set of multipliers was applied.

4.0 Data Analysis

4.1 Image Analysis

Eleven water vapor bands near 1400 and 1900 nm and two other bands considered to be noisy were excluded from image analysis. The remaining 115 bands of RTGC-corrected image reflectance data were further reduced with the ENVI (Environment for Visualizing Images) Minimum Noise Fraction (MNF) transformation to 20 MNF bands. The MNF transformation segregates the noise from the data resulting in a reduced number of bands containing the most meaningful information. Mixture Tuned Matched Filtering (MTMF) partial-unmixing algorithm (ENVI, 2004) was applied to the 20 MNF-transformed bands on all 14 flight lines of image data (Boardman, 1998). A library of reference spectra representing ash, bare soil, and scorched and green vegetation was created for each data cube for use in the unmixing process. The reference spectra extracted from flight line 7 (includes the Cheesman Reservoir calibration site) are shown in Figure 2. The MTMF algorithm suppresses the spectra of materials not included in the library spectra by processing them as background information.

All the libraries, one generated for each flight line, were transformed to MNF space using the same statistics file derived from the MNF transformation of the corresponding image (ENVI, 2004). By creating a different library for each image, the residual atmospheric effects (after the RTGC calibration) were present in both the library and the corresponding image data, minimizing their effect on the unmixing process. The disadvantage of this method is that a slightly different library was used for each data cube, reducing the consistency from one flight line to the next.

ENVI produces two gray-scale output images for each input spectrum: a matched filter score and an infeasibility value. The matched filter (MF) score, generally varying from 0 to 1, indicates how well the image pixel compares to the library reference spectrum and measures how abundant (ideally, a percentage) that material is in the image pixel. The infeasibility (IF) value shows how likely or unlikely the match is. In general, pixels that combine high MF scores with low IF values are a better match to the endmember spectrum (ENVI, 2004). Using a 2-D scatterplot of score versus infeasibility for the ash spectra (Figure 3), ENVI allows the user to interactively select pixels that best match the library reference spectrum. A mask was generated where high IF values occurred with high MF scores (i.e., false positives) to minimized the misidentification of ground components.

Once each data cube was unmixed, the resulting score and infeasibility images were georeferenced, and all the flight lines were combined into a single image mosaic. This image contained 8 continuous gray-scale bands: a score and IF band for each of the component spectra of ash, scorched vegetation, green vegetation, soil. The individual gray-scale fraction maps for each input endmember may be used individually or in any combination in a red-green-blue (RGB) color-composite image for simultaneous cover-type detection.

4.4 Statistical analysis of unmixing results relative to ground measurements

Detailed ground observations from 72 of the 183 sample plots (20 low, 26 moderate, and 26 high burn severity) were used to validate the image unmixing results. These 72

plots were near the center of flight lines where location errors were minimal (5 to 10 m or 1 to 2 pixels) as confirmed from the location/proximity of nearby road intersections. Because plot locations do not always center in a pixel, a 3 x 3 pixel area consisting of the 9 pixels adjacent pixels to the best-known plot location was analyzed for each plot. Each 9-pixel (15-m square) window was assumed to have homogenous burn characteristics. The mean MF scores of each of the four endmembers used to unmix the image were extracted from each pixel window at the selected plot locations. Because the MTMF routine is a partial unmixing process, the sum of the MF scores at each pixel was almost always less than one. A negative MF score was re-scored as zero to indicate the absence of the material within the plot/pixel.

Correlations between the measured ground values and the spectral abundance from the unmixing results (MF scores) were assessed for each endmember using the nonparametric Spearman test (SAS Institute Inc., 1999). Correlations were regarded as significant when p-value<0.05. Linear regressions with ground data as the independent variables and spectral data as the dependent variables were used to further examine the relationship between the ground and spectral data. For comparison to previous methods, both the MF scores from the spectral unmixing and the NBR values from the original BAER burn severity map were used as spectral data in the regressions. Adjusted R^2 (Adj. R^2) and root mean square error (RMSE) terms were reported from the regressions.

The population distributions of both the ground data and the MF scores were skewed left as indicated by an abundance of zeros, therefore, non-parametric statistics were used to test the similarity of the data distributions (Devore, 2000). The Wilcoxon Rank Sum

test was used to test the statistical difference in location of the medians of the distributions of the ground data versus the MF scores for each endmember (Devore, 2000). *P*-values>0.05 indicate no significant difference between median locations, however, since it is not statistically correct to accept the null hypothesis, 90% confidence intervals (lower and upper limits) were calculated to determine the statistical difference in medians between the two data sets. A kernel density estimator (bandwidth=1.06 times standard deviation) (Scott, 1992) was used to graphically compare the distributions of the ground data versus the MF scores for each input endmember. Kernel density estimators are nonparametric, smooth the data and facilitate the detection of characteristics such skewness, outliers and multi-modality.

5.0 Results and Discussion

5.1 Comparison of unmixing results with ground measurements

The MF scores were overall representative of the ground-based measures of ash, soil, scorched and green vegetation (Table 1), and were more indicative of the presence of a material, rather than the exact quantity. The presence of ash was spectrally detected 59% of the time, scorched and green vegetation were detected 72 and 71% of the time, respectively, and at least a trace of soil was spectrally detected 93% of the time. The positive relationship between the ground measurements and the MF scores indicated that as more of a material was measured on the ground, the MF scores increased as well. Thus, the means and medians of the measured ground values were generally higher than the corresponding MF scores.

The significant correlations between ground measurements and MF scores of scorched (r=0.55) and green (r=0.51) vegetation from the unmixing results can be attributed to the relative ease of measuring the canopy vegetation with an airborne sensor (Table 2). Ash (r=0.29) and soil (r=0.40) were more weakly correlated to MF scores because vegetation often occludes the surface from the sensor. We observed positive correlations between ash and soil variables and negative correlations between these variables and green or scorched vegetation. Ash and soil are often found together in burned areas; ash alone (red) or ash and soil mixed (purple) are indicative of areas that were burned at high severity (Figure 4). Scorched and green vegetation are also likely to be found together, in areas burned either at moderate or low severity (Figure 4).

The results from the linear regressions (Table 3) show that the ground and MF scores for all four endmembers were related statistically. A high Adj. R^2 value combined with a low RMSE term indicates a good fit between the two data sets. As was found with the correlation analysis, the strongest relationship between the ground data and MF scores was from the green vegetation (Adj. R^2=0.63, RMSE=4), while ash had the weakest relationship (Adj. R^2=0.08, RMSE=13).

When the ground data were regressed with the corresponding NBR values (Table 4), it was apparent these were weaker relationships than with the MF scores (Table 3). The statistically significant regression fits were between the NBR values and the ground measured soil (Adj. R^2=0.19), scorched vegetation (Adj. R^2=0.12) and green vegetation (Adj. R^2=0.05) (Table 4). We anticipated the strong correspondence with soil and

expected a similar relationship for the green vegetation because of the constitution of the NBR values.

Stronger regression fits between the ground data and MF scores compared to the NBR values indicates that spectral unmixing improves the identification of postfire ground measures. There is a greater ability to predict all four ground measures with MF scores than with NBR values. The ability to identify postfire ash cover is perhaps the most significant improvement over previous mapping methods. Ash cover is indicative of complete vegetation combustion (Smith *et al*., 2005), and often the most severely burned areas of a fire.

The Wilcoxon Rank Sum distribution analysis showed that the population distribution of the ground measures of green vegetation (p-value=0.4) was not significantly different than the corresponding distribution of MF scores (Figure 5d). Small p-values for all other distributions indicate they were significantly different. The difference in the median green vegetation observed from the ground data (8%) and the median spectral abundance of green vegetation from the unmixing results (5%) is small (Table 1, Figure 5d). The distributions of ash ground and MF scores were statistically different, yet the kernel density estimator fit similar lines to the two data sets and the difference in medians was also small (3%). These results (Figure 5a) indicate greater similarities between the ash ground and MF scores that were weakly identified with the correlation or regression analysis. Thus, a range of analysis techniques allows for added information regarding the relationships between the two data sets.

Overall, the relative spectral abundance (MF scores) of each of the endmembers, ash, soil, scorched and green vegetation, were well matched with the measured ground data. The hyperspectral data were acquired two months after the fire was controlled and during that time a few storms caused runoff and erosion, which changed surface conditions by redistributing ash and fine litter. Stronger relationships may have been found if the ground data and image data were collected at similar times. The lack of precise georegistration of the image also made it difficult to compare the field spectra and ground data to the exact pixels in the hyperspectral image.

5.2 Postfire map

The RGB (red, green, blue) color composite (Figure 4) created from the unmixing results identifies and quantifies postfire ash cover, scorched vegetation and soil cover. The spectra used as endmembers can be used to relate the fire-induced physical changes of the surface which are indicative of the fire's effect on the soil. Regions that are at the greatest risk of erosion are the areas where all vegetative ground cover has been removed by the fire, i.e., ash or soil cover. In Figure 4, ash is indicated by red while exposed soil is a blue color, mixing the two results in a purple or magenta color. Areas with either of these characteristics were classified as high burn severity; both are highlighted on Figure 4. Scorched vegetation is green in Figure 4 and often occurs in transition areas around patches of complete vegetation combustion (ash). Moderate severity areas are characterized by scorched vegetation; however, they are also typically heterogeneous and usually have patches of both ash and green vegetation (Figure 4).

Green vegetation is not shown directly on the postfire map because only three colors could be used and because there was little green vegetation remaining within the fire perimeter. The unburned areas are identifiable, however, just outside of the prominent region of ash and scorched vegetation (Figures 4). Low burn severity is more difficult to recognize than either high or moderate burn severity. Areas next to or surrounded by scorched vegetation that are not red or orange can be classified as low burn severity. These regions are mostly darker (brownish) in color and many have soil pixels (blue) mixed in. The natural vegetation in the region is sparse in many areas the granitic soil is easily seen between the trees.

Fire effects on the ground surface, such as changes in the surface vegetation and unconsumed litter, mineral soil and root conditions, are not always visible from above the canopy. Surface-level features may also be covered by residual ash, making it difficult for a non-ground-penetrating remote sensor to image the relevant data. For example, the amount of postfire litter, i.e., remaining fallen needles, woody debris, organic material, covering the mineral soil is an important indicator of burn severity and potential watershed response that is often covered by ash or masked by unburned tree canopy. Consequently, it is difficult to assess burn severity and other related factors, such as erosion potential, with a single, postfire imaging tool. However, the integration of several sources of data, including the results of reflectance spectral image analysis, may expedite and refine the information that guides postfire stabilization and rehabilitation efforts.

5.3 Hyperspectral image data considerations

The analytical results of this project indicate that hyperspectral image data are useful to evaluate forested areas after wildfire. However, if this information is to be used to assist in postfire rehabilitation decisions, then timely data acquisition and analysis are essential. Within this project, several operational issues became apparent: 1) Because of logistical and safety concerns and the presence of smoke, image data are not easily acquired immediately during a fire, however rapid response of image acquisition and data processing is essential if the image is to be used by BAER teams (Orlemann *et al*., 2002). 2) In areas requiring large coverage, efforts must be made to maintain data quality and consistency between flight lines (Aspinall *et al*., 2002). 3) Metadata that documents the data processing steps is needed to detect problems with the data. 4) Because of the large data files involved, the data pre-processing and the format of the product data files needs to be specified. In addition to the general operational issues previously described, the analysis of the data for this study required the generation of an individual reference library for each flight line to deal with data inconsistencies resulting in a final mosaic that was not entirely "seamless."

6.0 Conclusions

The materials discrimination power of hyperspectral imagery allowed us to characterize postfire materials represented in a pixel and quantify the physical abundance in a corresponding ground location. The unmixed image identified the relative abundance of four ground components (ash, soil, scorched and green vegetation) that we determined to be important for determining and classifying burn severity. The measured ground

value of each component/endmember was significantly related to the corresponding spectral MF scores based on an assessment of 72 validation field plots. The additional information provided by the fine scale hyperspectral imagery makes it possible to more accurately assess the effects of the fire on the soil surface as compared to NBR values derived from satellite imagery. These surface effects, especially ash and soil cover, are more indicative of potential watershed response.

Unique libraries of reference spectra were used to unmix each of the data cubes; therefore, it is likely that the libraries themselves may only be useful on future fires in ponderosa pine and Douglas fir habitat on similar soils, thus limiting their usefulness. However, the spectral endmembers that were used in the unmixing were representative of burn severity and were abundant on the study plots within the image. These same endmembers should be used in the future to unmix images and classify burn severity. Additional research is needed to develop an analytical procedure that can be used repetitively between flight lines and, ideally, between fires.

References

Adams, J. B., Smith, M. O., and Johnson, P. E., 1986. Spectral mixture modeling: a new analysis of rock and soil types at the Viking Lander 1 site, *Journal of Geophysical Research*, 91(B8):8098-8112.

Adams, J. B., Sabol, D. E., Kapos, V., Filho, R. A., Roberts, D. A., Smith, M. O., and Gillespie, A. R., 1995. Classification of multispectral images based on fractions of endmembers: application to land-cover change in the Brazilian Amazon, *Remote Sensing of Environment*, 52:137-154.

Analytical Imaging and Geophysics LLC, 2002. ACORN 4.0 stand-alone version, Analytical Imaging and Geophysics LLC, Boulder, Colorado, 64 p.

Aspinall, R. J., Marcus, W. A., and Boardman, J. W., 2002. Considerations in collecting, processing, and analyzing high spatial resolution hyperspectral data for environmental investigations, *Journal of Geographical Systems*, 4:15-29.

Boardman, J. W., 1998. Leveraging the high dimensionality of AVIRIS data for improved subpixel target unmixing and rejection of false positives: mixture tuned matched filtering, *Summaries of the Seventh Annual JPL Airborne Earth Science Workshop* (R.O. Green, editor), 12-16 January 1988, Pasadena, California (California Institute of Technology, Pasadena, California), Vol. 1, 55 p.

Clark, J., Parsons, A., Zajkowski, T., and Lannom, K., 2003. Remote sensing imagery support for burned area emergency response teams on 2003 Southern California Wildfires, U.S. Department of Agriculture Forest Service, Remote Sensing Applications Center, Report No. RSAC-2003-RPT1, Salt Lake City, Utah, 18 p.

Clark, R. N., Swayze, G. A., Livo, K. E., Kokaly, R. F., King, T. V., Dalton, J. B., Vance, J. S., Rockwell, B. W., Hoefen, T., and McDougal, R. R., 2002. Surface reflectance calibration of terrestrial imaging spectroscopy data: a tutorial using AVIRIS, AVIRIS workshop proceedings, URL: http://popo.jpl.nasa.gov/pub/docs/workshops/02_docs/2002_Clark_web.pdf, (last date accessed: 12 August 2004).

Cipra, J. E., Kelly, E. F., MacDonald, L., and Norman, J., 2003. Ecological Effects of the Hayman Fire part 3: soil properties, erosion and implications for rehabilitation and aquatic ecosystems, *Hayman Fire Case Study Analysis* (R.T. Graham, editor), U.S. Department of Agriculture Forest Service, General Technical Report RMRS-GTR-114, Rocky Mountain Research Station, Fort Collins, Colorado, pp. 204-219.

Colorado Climate Center, 2004. Colorado Climate Center data access, URL: http://climate.atmos.colostate.edu/dataaccess.shtml, Colorado State University, Ft. Collins, Colorado (last date accessed: 25 February 2004).

DeBano, L. F., Neary, D. G., and Ffolliott, P. F., 1998. *Fire's Effects on Ecosystems*, John Wiley and Sons, New York, N.Y., 352 p.

DeBano, L. F., 2000. The role of fire and soil heating on water repellency in wildland environments: a review, *Journal of Hydrology*, 231-232:195-206.

Devore, J. L., 2000. *Probability and Statistics for Engineering and the Sciences*, Brooks/Cole, Pacific Grove, California, 775 p.

ENVI, 2004. The Environment for Visualizing Images Online Help, Version 4.1, Research Systems, Inc., Boulder, Colorado.

Gao, B. C., Heidebrecht, K. B., and Goetz, A. F. H., 1993. Derivation of scaled surface reflectances from AVIRIS data, *Remote Sensing of Environment*, 44:165-178.

Graham, R. T., technical editor, 2003. *Hayman Fire Case Study*, U.S. Department of Agriculture Forest Service, General Technical Report RMRS-GTR-114, Rocky Mountain Research Station, Fort Collins, Colorado, 404 p.

Hardwick, P., Lachowski, H., Maus, P., Griffith, R., Parsons, A., and Warbington, R., 1997. Burned Area Emergency Rehabilitation (BAER) Use of Remote Sensing, U.S.

Department of Agriculture Forest Service, Remote Sensing Applications Center, Report No. RSAC-001-TIP1, Salt Lake City, Utah, 4 p.

Ice, G. G., Neary, D. G., and Adams, P. W., 2004. Effects of wildfire on soils and watershed processes, *Journal of Forestry*, 102(6):16-20.

Jain, T. B., Pilliod, D. S., and Graham, R. T., 2004. Tongue-tied, *Wildfire*, July-August: 22-26.

Key, C. H., and Benson, N.C., 2002. The normalized difference burn ratio (NDBR): A Landsat TM radiometric measure of burn severity, URL: http://www.nrmsc.usgs.gov/research/ndbr.htm, U.S. Geological Survey, Northern Rocky Mountain Science Center, Montana State University, Bozeman, Montana (last date accessed: 12 April 2005).

Lewis, S. A., Wu, J. Q., and Robichaud, P. R., in press. Assessing burn severity and comparing soil water repellency, Hayman Fire, Colorado. *Hydrological Processes*.

Moody, J. A., Smith, J. D., and Ragan, B. W., 2005. Critical shear stress for erosion of cohesive soils subjected to temperatures typical of wildfires, *Journal of Geophysical Research*, 110(F1).

Moody, J. A., and Martin, D. A., 2001. Initial hydrologic and geomorphic response following a wildfire in the Colorado Front Range, *Earth Surface Processes and Landforms*, 26:1049-1070.

Orlemann, A., Saurer, M., Parsons, A., and Jarvis, B., 2002. Rapid delivery of satellite imagery for burned area emergency response (BAER), *Proceedings of the Ninth Biennial Forest Service Remote Sensing Applications Conference*, 8-12 April 2002, San Diego, California, unpaginaged CD-ROM.

Parsons, A. 2003. Burned area emergency rehabilitation (BAER) soil burn-severity definitions and mapping guidelines, U.S. Department of Agriculture Forest Service, Remote Sensing Applications Center, Report No. RSAC-2003-RPT1, Salt Lake City, Utah, 9 p.

Parsons A., and Orlemann A., 2002. Mapping post-wildfire burn severity using remote sensing and GIS, 2002 ESRI International User Conference, 8-12 July 2002, San Diego, California, 9 p.

Patterson, M. W., and Yool, S. R., 1998. Mapping fire-induced vegetation mortality using Landsat Thematic Mapper data: a comparison of linear transformation techniques, *Remote Sensing of Environment*, 65:132-142.

Roberts, D. A., Smith, M. O., and Adams, J. B., 1993. Green vegetation, nonphotosynthetic vegetation and soils in AVIRIS data, *Remote Sensing of Environment*, 44:255-269.

Robichaud, P. R., 2000. Fire effects on infiltration rates after prescribed fire in Northern Rocky Mountain forests, USA, *Journal of Hydrology* 231-232:220-229.

Robichaud, P., MacDonald, L., Freeouf, J., Neary, D., Martin, D., and Ashmun, L., 2003, Postfire rehabilitation of the Hayman Fire, *Hayman Fire Case Study Analysis* (R.T. Graham, editor), U.S. Department of Agriculture Forest Service, General Technical Report RMRS-GTR-114, Rocky Mountain Research Station, Fort Collins, Colorado, pp. 293–313.

Romme, W. H., Veblen, T. T., Kaufmann, M. R., Sherriff, R., and Regan, C. M., 2003, Ecological Effects of the Hayman Fire Part 1: Historical (Pre-1860) and Current (1860 to 2002) Fire Regimes, *Hayman Fire Case Study Analysis* (R.T. Graham, editor), U.S. Department of Agriculture Forest Service, General Technical Report RMRS-GTR-114, Rocky Mountain Research Station, Fort Collins, Colorado, pp. 181–195.

RSAC, 2005. Remote Sensing Applications Center Burned Area Emergency Response (BAER) Imagery Support, URL: http://www.fs.fed.us/eng/rsac/baer/, U.S. Department of

Agriculture Forest Service, Remote Sensing Applications Center, Salt Lake City, Utah (last date accessed: 15 June 2005).

Ryan, K. C., 2002. Dynamic interactions between forest structure and fire behavior in boreal ecosystems, *Silva Fennica*, 36(1):13-39.

Ryan, K. C., and Noste, N. V., 1983. Evaluating prescribed fires, *Proceedings of the Symposium and Workshop on Wilderness Fire* (Lotan, J.E., Kilgore, B.M., Fischer, W.C., and Mutch, R.W., editors), U.S. Department of Agriculture Forest Service, General Technical Report INT-182, Intermountain Research Station, Ogden, Utah, pp. 230-238.

SAS Insititute Inc. 1999. *SAS/STAT User's Guide, Volume 1, Version 8.2*, Statistical Analysis Systems (SAS) Institute Inc., Cary, North Carolina.

Scott, D. W., 1992. *Multivariate Density Estimation: Theory, Practice, and Visualization*, John Wiley and Sons, Inc, New York, N.Y.

Smith, A. M. S., Wooster, M. J., Drake, N. A., Dipotso, F. M., Falkowski, M. J., Hudak, A. T., 2005. Testing the potential of multi-spectral remote sensing for retrospectively estimating fire severity in African Savannahs, *Remote Sensing of Environment* 97:92-115.

Song, C., 2005. Spectral mixture analysis for subpixel vegetation fractions in the urban environment: how to incorporate endmember variability?, *Remote Sensing of Environment*, 95:248-263.

Theseira, M. A., Thomas, G., Taylor, J. C., Gemmell, F., and Varjo, J., 2003. Sensitivity of mixture modeling to end-member selection, *International Journal of Remote Sensing*, 24(7):1559-1575.

van Wagtendonk, J. W., Root, R. R., and Key, C. H., 2004. Comparison of AVIRIS and Landsat ETM+ detection capabilities for burn severity, *Remote Sensing of Environment*, 92:397-408.

Table Captions

Table 1. Means, medians, ranges and standard deviations of the measured ground cover and spectral values (MF scores) of each endmember classified by soil burn severity.

Table 2. Correlation matrix of *r*-values between ground values and spectral values (MF scores). *P*-values are in parenthesis; bold correlations are significant at $p<0.05$; $n=72$.

Table 3. Linear regression coefficients, ground values versus MF scores; MF score is the dependent variable ($n=72$). *P*-values are considered significant at $p<0.05$ and are in bold.

Table 4. Linear regression coefficients, ground values versus NBR value; NBR value is the dependent variable ($n=72$). *P*-values are considered significant at $p<0.05$ and are in bold.

List of Figures

Figure 1. BAER burn severity map of Hayman Fire. Transect locations and an example plot layout are shown.

Figure 2. Spectral reflectance plot of four endmembers that were used in the MTMF unmixing process.

Figure 3. Scatterplot of ash matched filter (MF) scores versus ash infeasibility (IF) values from the results of the image unmixing.

Figure 4. Red, green, blue (RGB) color composite of the unmixed image. Red pixels represent ash cover, green pixels represent scorched vegetation and blue pixels represent soil cover. High burn severity (A) is characterized by nearly complete ash coverage, while (B) is a mix of ash and soil. Moderate burn severity is characterized by scorched vegetation; low burn severity and unburned areas are characterized by green vegetation, within and outside of the fire perimeter, respectively.

Figure 5. Kernel density estimates comparing the population distributions of the measured ground data and the spectral matched filter scores for each endmember: a) ash; b) soil; c) scorched vegetation; and d) green vegetation. Wilcoxon p-values<0.05 indicate significant differences between the two data sets; similar distribution shapes and small 90% confidence interval differences between medians indicate similarities.

Table 1.

	Ground cover (%)				MF scores			
	Mean	Median	Range	Std.	Mean	Median	Range	Std.
Low soil burn severity (*n*=20)								
Ash cover	8	5	0–40	10	2	0	0–17	4
Soil cover	20	10	1–70	22	2	2	0–7	2
Scorched vegetation	56	56	0–100	35	23	16	5–55	16
Green vegetation	25	29	0–52	15	13	16	0–24	8
Moderate soil burn severity (*n*=26)								
Ash cover	13	10	0–50	12	13	4	0–67	17
Soil cover	52	51	5–95	25	8	5	0–28	8
Scorched vegetation	42	34	6–100	26	21	14	0–69	22
Green vegetation	2	1	0–17	3	2	1	0–10	3
High soil burn severity (*n*=26)								
Ash cover	19	20	0–70	17	15	12	0–43	13
Soil cover	70	74	16–94	21	13	13	0–30	8
Scorched vegetation	23	22	6–53	11	4	0	0–55	12
Green vegetation	0	0	0–1	0	2	1	0–9	3
All data (*n*=72)								
Ash cover	10	14	0–70	14	4	11	0–67	14
Soil cover	53	50	1–95	30	5	8	0–30	8
Scorched vegetation	29	39	0–100	28	8	15	0–69	19
Green vegetation	1	8	0–52	13	3	5	0–24	7

Table 2.

	Ash spectra	Soil spectra	Scorch spectra	Green spectra
Ash ground	**0.30 (0.01)**	0.05 (0.66)	-0.21 (0.08)	-0.21 (0.07)
Soil ground	**0.33 (0.005)**	**0.40 (0.0006)**	**-0.50 (<0.0001)**	**-0.38 (0.001)**
Scorch ground	-0.18 (0.13)	-0.17 (0.17)	**0.55 (<0.0001)**	0.14 (0.24)
Green ground	**-0.48 (<0.0001)**	**-0.40 (0.0004)**	**0.43 (0.0001)**	**0.51 (<0.0001)**

Table 3.

	RMSE (%)	Adj. R^2	*p*-value
Ash cover	13	**0.08**	**0.01**
Soil cover	7	**0.22**	**<0.0001**
Scorched vegetation	15	**0.33**	**<0.0001**
Green vegetation	4	**0.63**	**<0.0001**

Table 4.

	RMSE (%)	Adj. R^2	*p*-value
Ash cover	214	0.01	0.78
Soil cover	191	**0.19**	**<0.0001**
Scorched vegetation	199	**0.12**	**0.002**
Green vegetation	208	**0.05**	**0.03**

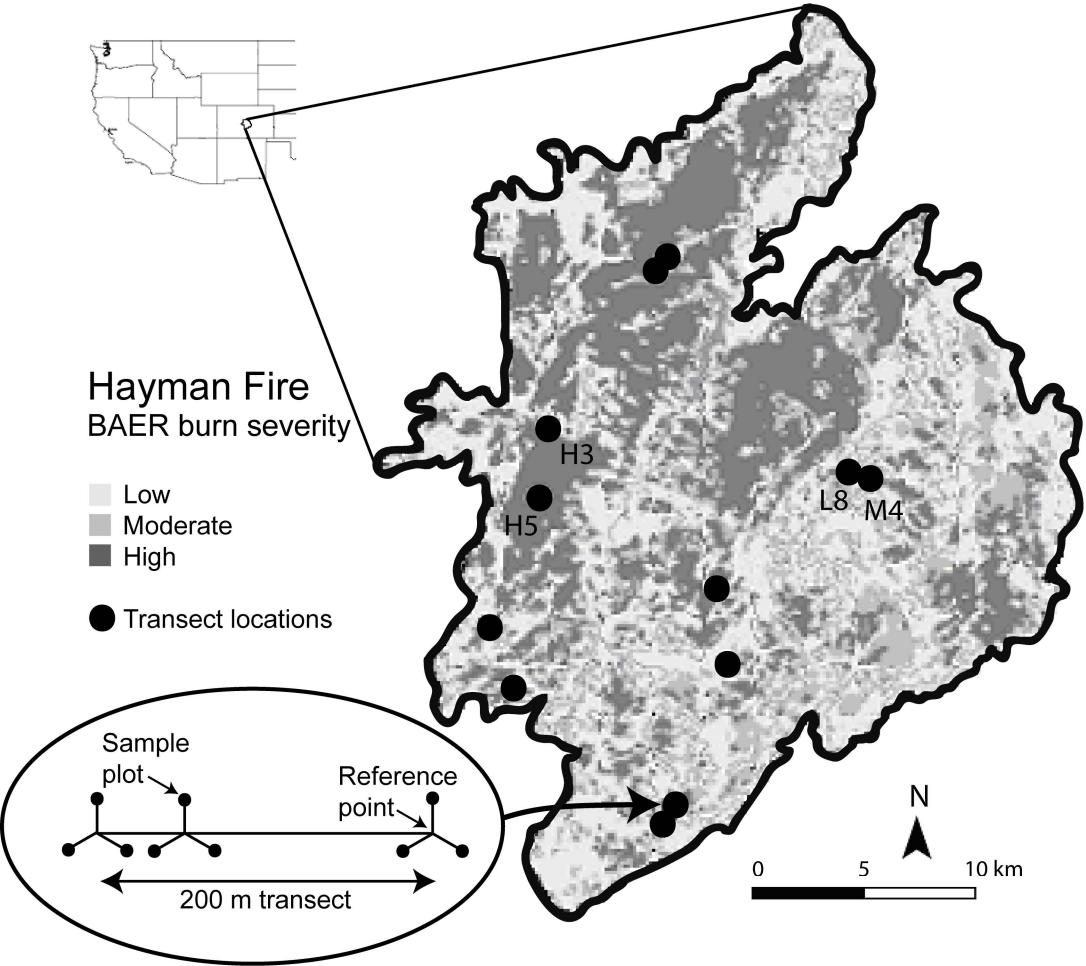
Hayman Fire
BAER burn severity
Low
Moderate
High
Transect locations
H3
H5
L8
M4
Sample plot
Reference point
200 m transect
N
0
5
10 km

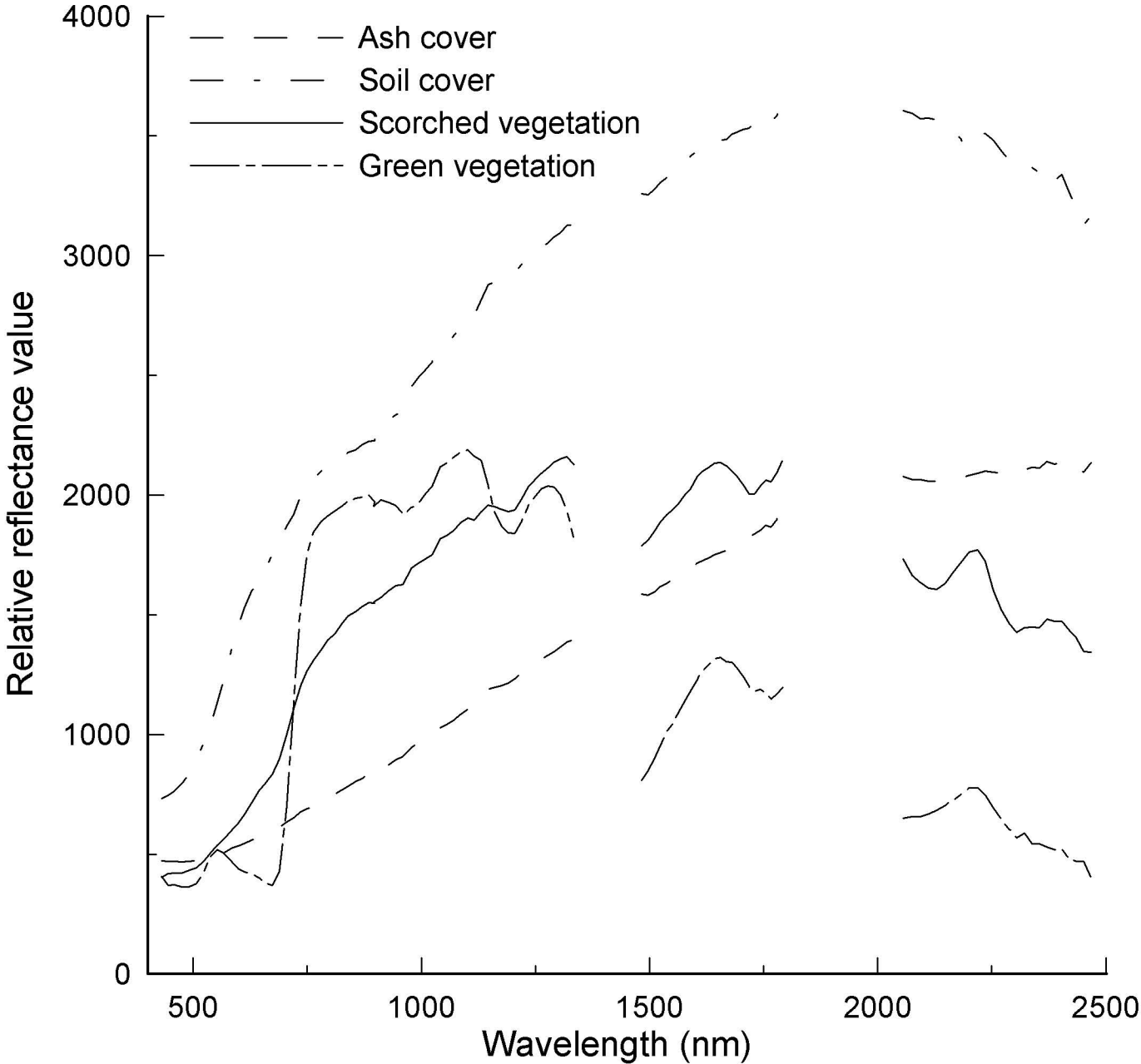
Ash cover
Soil cover
Scorched vegetation
Green vegetation
Relative reflectance value
4000
3000
2000
1000
0
500
1000
1500
2000
2500
Wavelength (nm)

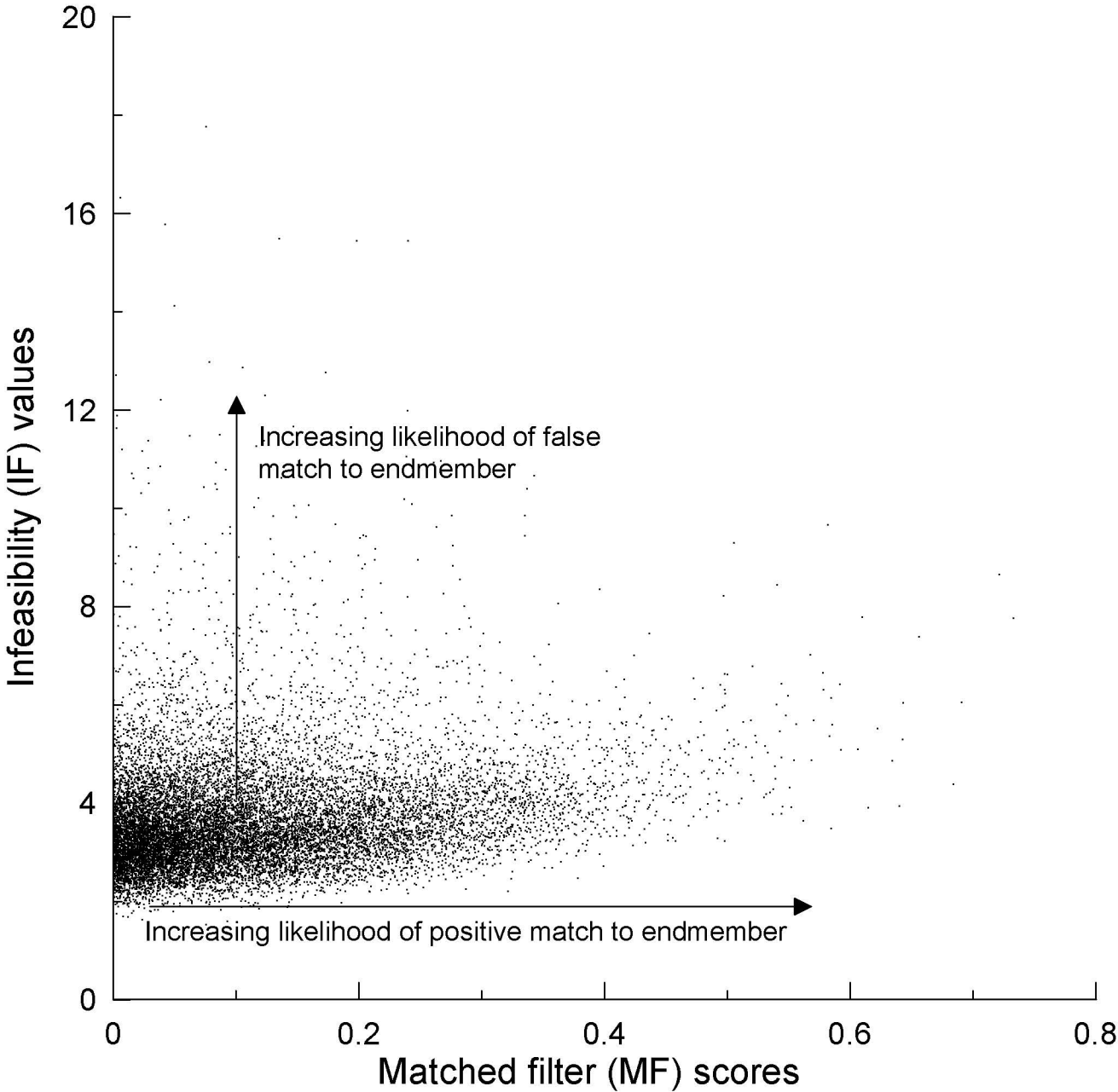
20
16
12
8
4
0
Infeasibility (IF) values
Increasing likelihood of false match to endmember
Increasing likelihood of positive match to endmember
0
0.2
0.4
0.6
0.8
Matched filter (MF) scores

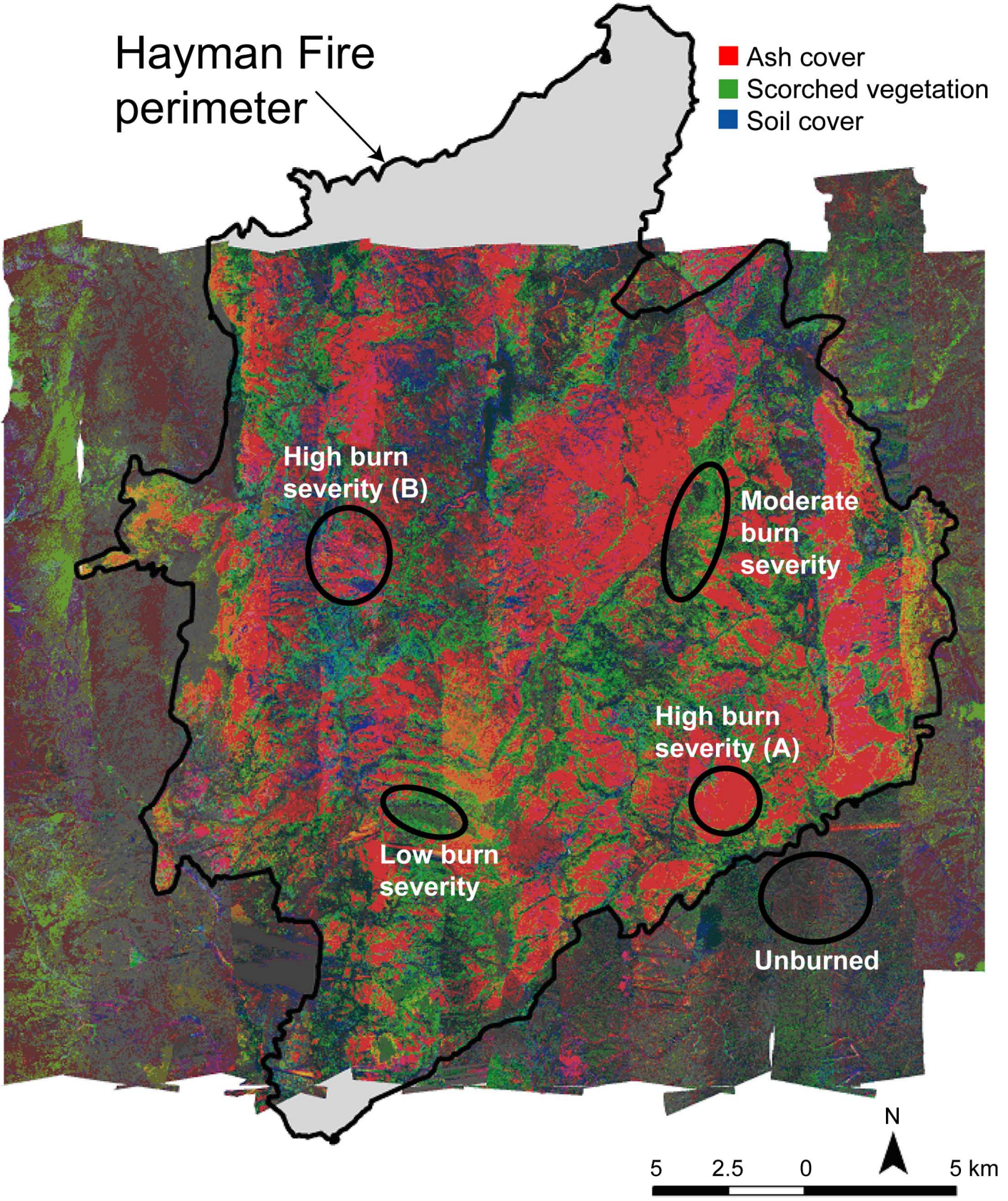
Hayman Fire perimeter
Ash cover
Scorched vegetation
Soil cover
High burn severity (B)
Moderate burn severity
High burn severity (A)
Low burn severity
Unburned
N
5
2.5
0
5 km

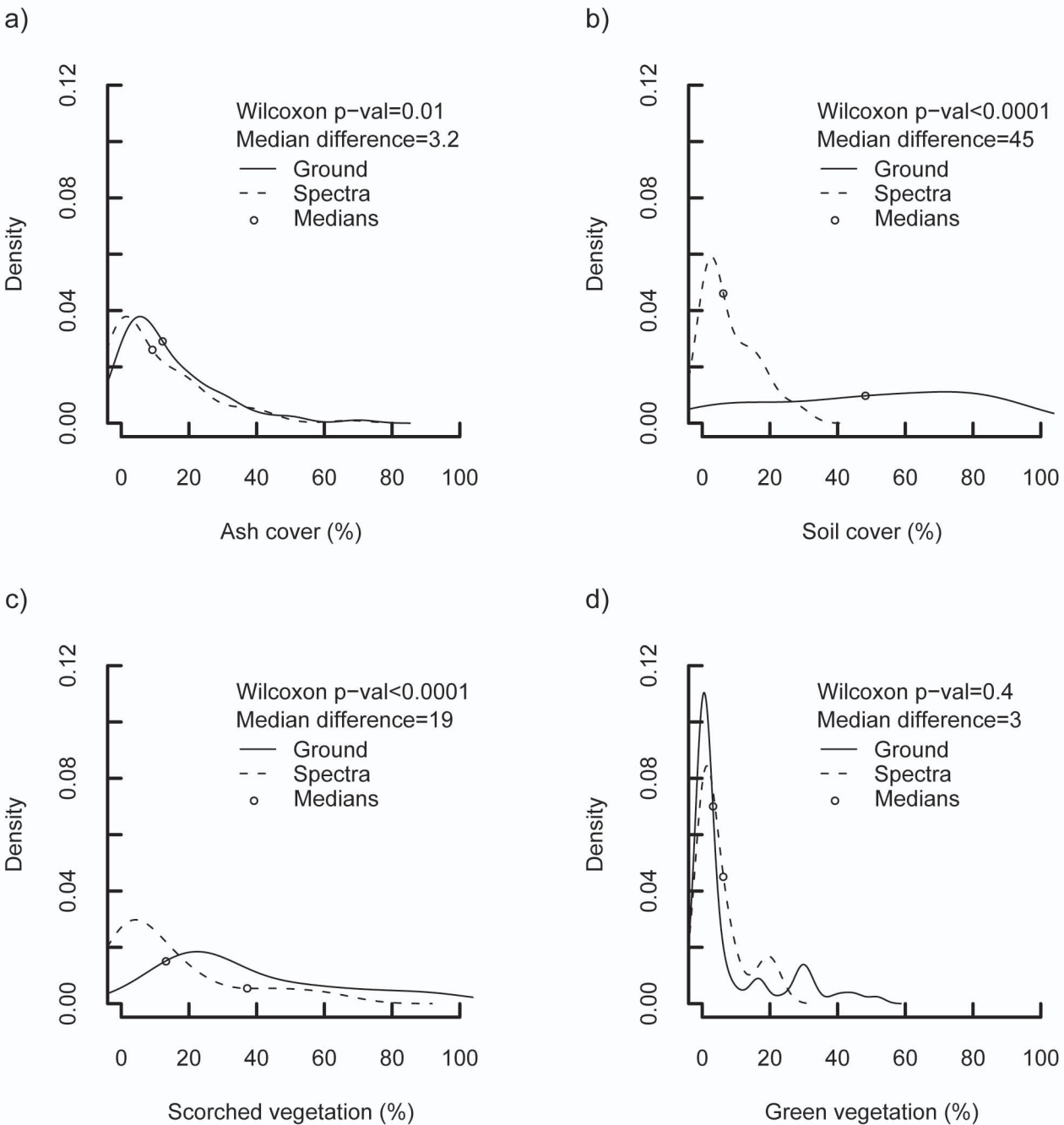
a)
Wilcoxon p−val=0.01
Median difference=3.2
Ground
Spectra
Medians
Density
0.00
0.04
0.08
0.12
0
20
40
60
80
100
Ash cover (%)
b)
Wilcoxon p−val<0.0001
Median difference=45
Ground
Spectra
Medians
Density
0.00
0.04
0.08
0.12
0
20
40
60
80
100
Soil cover (%)
c)
Wilcoxon p−val<0.0001
Median difference=19
Ground
Spectra
Medians
Density
0.00
0.04
0.08
0.12
0
20
40
60
80
100
Scorched vegetation (%)
d)
Wilcoxon p−val=0.4
Median difference=3
Ground
Spectra
Medians
Density
0.00
0.04
0.08
0.12
0
20
40
60
80
100
Green vegetation (%)